Validation of a Convection Scheme using TRMM data

Andreas Rhodin

Max-Plank-Institute for Meteorology, 20146 Hamburg, Germany

1. Introduction

The TRMM satellite is dedicated to observations of precipitation in the tropics. Besides others it carries an active precipitation radar (PR) to retrieve vertical profiles and passive microwave radar (TMI). The TRMM precipitation estimates from a 2 weeks period in August/September 1998 are used to evaluate the precipitation rates from the mesoscale model REMO. TRMM data from NASA/NASDA as well as alternative retrieval products from the partners of the EuroTRMM project were used for the study.

In order to evaluate the physical parameterizations of the mesoscale model REMO, a case study over the Pacific atoll region was carried out to allow comparison with rain-gauge data as well. This case study is characterized by almost stationary large scale conditions. Total rainrates (temporal and spatial mean), spatial distributions (temporal mean), histograms of rain rates intensities as well as profiles are compared to the results of different model runs.

2. REMO model description

REMO is a hydrostatic mesoscale model with 1/2° (used here) or 1/6° grid size and 19 vertical levels. The dynamical core is that of the former regional forecast model EM/DM of the German weather service DWD and the physical parameterizations are taken from the global circulation model ECHAM4 (Roeckner et al. 1996) of the Max Plank Institute for Meteorology (MPI). The parameterizations relevant to the simulation of rainfall are the convection parameterization based on a mass-flux approach (Tiedtke, 1989) and the parameterization of large scale precipitation based on an approach of Sundquist (1978).

2.1 Convection Parameterization: Mass Flux Approach

The convection parameterization is based on the work of Tiedtke (1989) with some extensions due to Nordeng (1994) . Here the parameterization is described briefly with emphasis on the parts relevant to the sensitivity studies.

2.2 Updrafts

The bulk equation for the mass of the ensemble of cumulus updrafts within a model column is

$$\frac{\partial}{\partial z} M_U = E_U - D_U \tag{1}$$

E and D denote the entrainment and detrainment rates. The bulk equations for $x=q$ (humidity), $x=s$ (heat) and $x=l$ (cloud water) are

$$\frac{\partial}{\partial z}(M_U x_U) = E_U x_E - D_U x_U + S \tag{2}$$

S denotes additional source and sink terms due to condensation, evaporation and rainfall. The subscripts $_U$ and $_E$ refer to quantities in the updraft or environment. The effect of cumulus convection on the large scale budget equations is given by the tendencies:

$$\frac{\partial x_E}{\partial t} = \frac{1}{\rho_\rho}\frac{\partial}{\partial z}[M_U x_U + M_D x_D - (M_U + M_D)x_E] + C \tag{3}$$

C denotes terms due to evaporation of rain in the unsaturated sub-cloud layer. The effect of downdrafts (M_U) are considered as well.

2.3 Precipitation Rates

The profiles of rain rates $\boldsymbol{P}$ are diagnosed from

$$P(z) = \int (G_p - w + m)\rho_\rho \partial z \tag{4}$$

with a similar equation for snow fall rates. G_P denotes the conversion rate from cloud water or ice, e evaporation or sublimation, and m melting. The conversion rates are parameterized as follows:

$$\rho_E G_P = 2 \bullet 10^{-3} m^{-1} \quad \text{if} \quad z > \quad z_B + \delta z_b, \quad \text{else} \quad 0 \tag{5}$$

z_B is the cloud base height and $\delta z_B = 1500$ m (over sea) is a parameter which prevents shallow cumulus clouds from raining.

2.4 Entrainment and Detrainment rates

Entrainment and detrainment rates are split into a part caused by turbulent exchange [1] and organized in- and outflow [2]. The turbulent part is parameterized as

$$E_U^{(1)} = \varepsilon_U M_U,\ D_U^{(1)} = \delta_U M_U,\ \text{with}\ \varepsilon_U = \delta_U = 1 \times 10^{-4} m^{-1}\ \text{(for penetrative convection).} \tag{6}$$

According to Nordeng (1994) the parameterization of organized entrainment is based on buoyancy, the fraction of organized detrainment between the level z_D (where clouds start to detrain) and z_T (the highest possible cloud level) is prescribed as a functional relationship.

2.5 Closure

So far entrainment and detrainment rates have been prescribed as a fraction of the mass flux M. The total mass-flux remains to be determined by specifying the mass flux at cloud base. This is done by a CAPE closure. Available potential energy (CAPE) is defined as

$$\text{CAPE} = \int_{\text{BASE}}^{\text{TOP}} \left(\frac{g}{T_{VE}}[T_V - T_{VE}] - gl\right)\partial z \tag{7}$$

For virtual temperature T_V and gravity acceleration g. The dominant part of the convective heating in Equation (3) is due to the compensating subsidence

$$\frac{\partial T_E}{\partial t} \approx \frac{1}{\rho_E c_p} M \frac{\partial}{\partial z} s_E \tag{8}$$

The total mass-flux is determined by demanding

$$\frac{\partial}{\partial t}\mathrm{CAPE} = -\frac{\mathrm{CAPE}}{\tau} \tag{9}$$

with a relaxation time $\tau = 900$s.

The downdraft mass flux is assumed to be proportional to the updraft mass-flux.

2.6 Parameterization of Large Scale Precipitation

The large scale cloud scheme is based on an approach of Sundquist (1978). Prognostic variables are water vapour and cloud liquid water content. Diagnostic quantities are fractional cloud cover, fraction of cloud ice to cloud water and precipitation rates.

2.7 Parameterization of Turbulent Fluxes from the Surface

The formulation of the lower boundary condition, i.e. of the turbulent fluxes at the surface, has strong influence on the latent heat release in cumulus convection. The fluxes for a variable x at the surface is calculated according to the bulk transfer relation:

$$\overline{(w'x')} = -C_X |v_L| (x_L - x_s) \tag{10}$$

w and v denote vertical and horizontal wind speed, $_L$ and $_S$ denote the lowest model level and the surface. C_X is the transfer coefficient defined according to Louis (1979). For low wind speeds this relation does not hold. Therefore, in unstable conditions over sea, an empirical interpolation is used between the free convection limit and the neutral approximation C_N (Miller et al., 1992):

$$C_X = C_N (1 + C_R^{\gamma})^{1/\gamma} \text{ with } C_R = \beta \frac{(\Theta_{VS} - \Theta_{VL})^{1/3}}{C_N |V_L|}, \quad \beta = 0.0016, \quad \gamma = 1.25 \tag{11}$$

3. Case Study

The REMO model has been run in four domains (cf. Figure 1) of 40°×40° with 1/2° resolution and 19 vertical levels for the period from August 15, 1998 to September 1. This period corresponds to that of the CAMEX field experiment. In addition to the NASA/NASDA 2A12 and 2A25 rain rate estimates the products of the EuroTRMM project partners were available during this time. Comparison with observations was started at August 18 to allow for a spin-up of clouds and precipitation. Initial and boundary conditions for the regional model runs were taken from the operational ECMWF analyses.

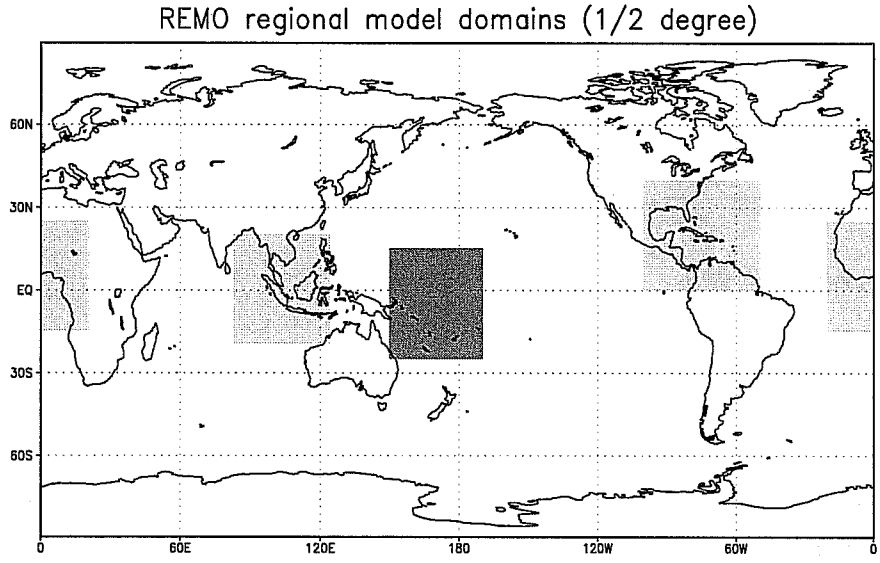

Figure 1: Location of the REMO model domains. The dark shaded Pacific atoll region is considered here.

3.1 Atoll Region

At the MPI models are run for climate research purposes. No data assimilation facilities are used in order to keep the model trajectories close to the observed weather. Besides climatological studies, only short time runs (not longer than a few days) can be compared directly with the observations. In order to do this for longer time periods the evolution within the model domain must be driven mainly by the boundary conditions and not by internal dynamics. This may be the case in higher latitudes, there depressions move through the model domain within a few days, but hardly in the tropics, there the exact location of cloud cluster development is hardly predictable.

Emphasis of the investigation was put on the Pacific atoll region for the following reasons:

- This region is located mostly over sea there TRMM estimates are supposed to be more accurate than over land. The convection parameterization is tested under well controlled conditions.
- The atoll islands host a number of rain gauge stations which provide a rainfall estimate independent from the satellite observations.
- The synoptic situation is characterized by a split tropical convergence zone which is quite stable over the period of investigation. Thus a statistical comparison of model results and observations is possible.

3.2 Coverage and Aggregation of Data

Figure 2 shows a typical coverage of the REMO domain with rain gauge stations and satellite over-passes during a 3 hours time period. The snapshot shows that the exact locations of high rain rates cannot be predicted by the model so that only a statistical comparison is feasible. The rain rate estimates from TRMM resolve a finer scale (4 km in case of PR and 21 km in case of TMI) than the regional model (approx. 55 km). Thus the satellite estimates have been aggregated to the model grid for the comparisons presented below. For each model grid-points all the satellite observations nearest to it were averaged.

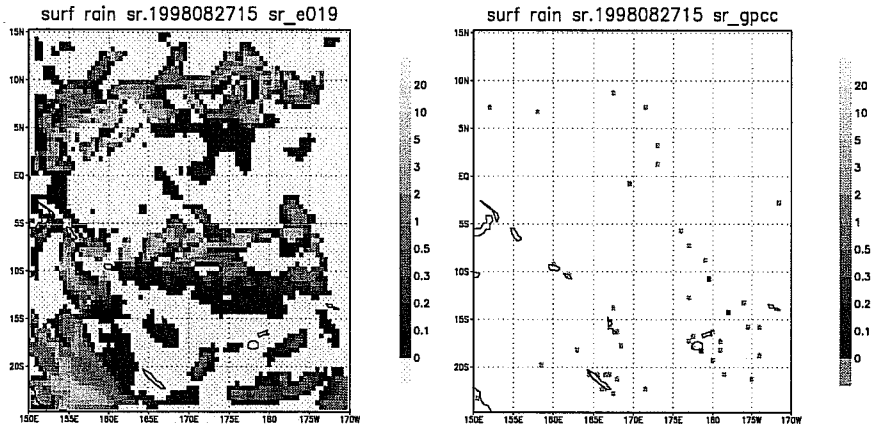

a) REMO Regional model run, 3 hourly accumulated surface precipitation [mm/h]

b) SYNOP rain gauge measurements [mm/h].

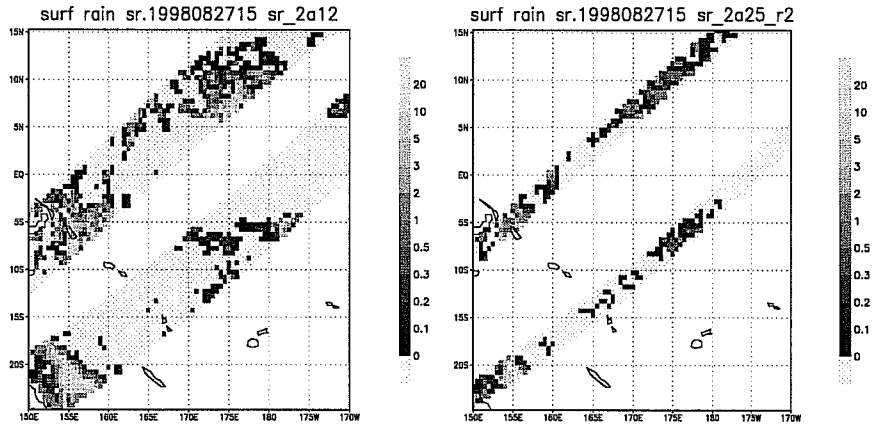

c) TRMM TMI derived surface rain rates (2A12) [mm/h].

d) TRMM PR derived surface rain rates (2A25) [mm/h].

Figure 2: Data coverage for a 3 hours period (27.8.1998, 12 to 15 UT). TRMM products are averaged to the model grid ($1/2^o$) before comparison for all results presented here.

3.3 Spatial Distributions

Figure 3 shows the spatial distribution of precipitation averages for the period from 1998-08-18 to 1998-09-01 (14 days). The distribution of REMO model precipitation rates (Figure 3a) compares well with those from TRMM TMI and PR. REMO rain rates are generally higher than TMI and PR rain rates. Near to the boundaries of the model domain, rain rates can not be compared due to boundary effects. Especially in the neighborhood of the eastern boundary, which provides inflow boundary conditions for the lower troposphere, much less precipitation occurs than in the inner part of the domain. This is due to some kind of spin-up effect: Zero cloud water content is prescribed at the boundaries and the model clouds have to adapt before precipitation can occur.

TRMM TMI (Figure 3c) and especially TRMM PR (Figure 3d) show much more scatter than the REMO rain rates. This is due to the lower statistics because information on rain rates is provided only for the over-passes whereas REMO rain rates are averaged from every model time step (5 minute intervals). In Figure 3b instantaneous model rain rates at the end of each 3 hourly interval were averaged, taking only those grid-points which coincided with a TMI over-pass during the prevailing 3 hours period, in order to get similar

statistics as TRMM TMI. In this case the scatter of the averaged model rain-rates is even higher than that of the averaged TMI rain-rates. The reason for that is the bimodal distribution of model rain-rates.

TRMM PR shows lower rain-rates than TMI in areas of high precipitation but higher rain-rates in areas of low precipitation.

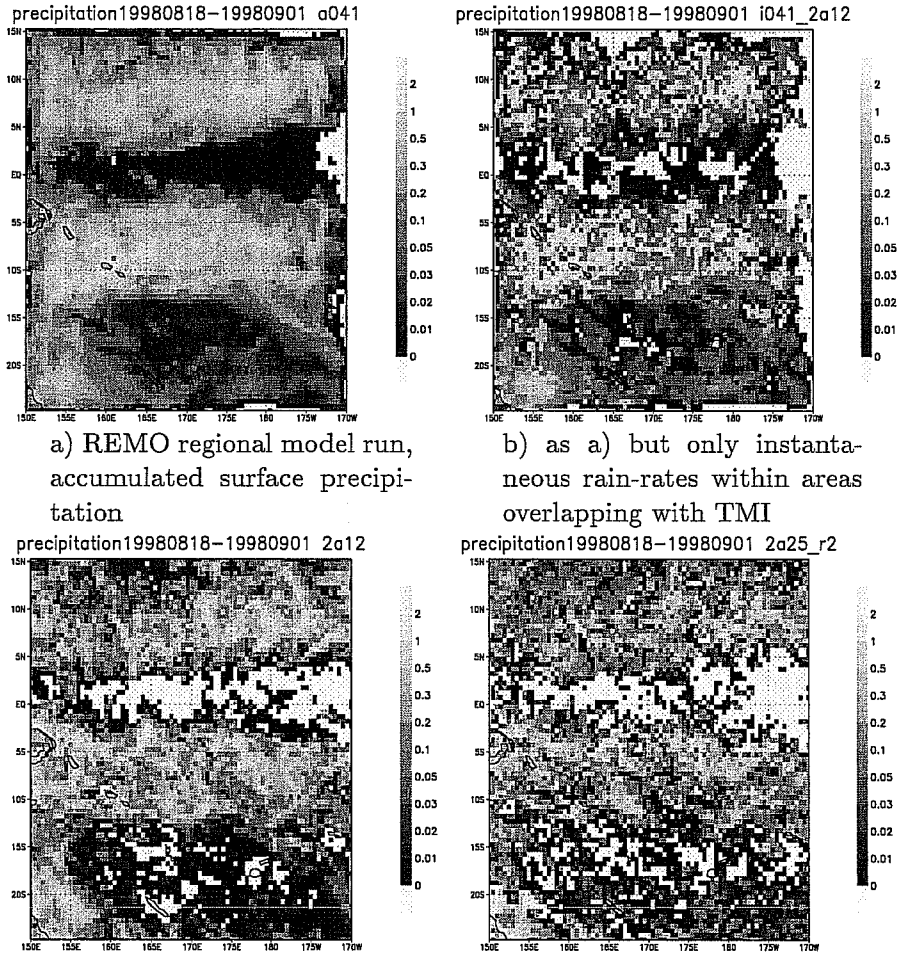

a) REMO regional model run, accumulated surface precipitation

b) as a) but only instantaneous rain-rates within areas overlapping with TMI

c) TRMM TMI (2A12) surface rain rates.

d) TRMM PR (2A25) surface rain rates.

Figure 3: Average rain rates [mm/h] from TRMM over-passes and 3 hourly model results, 1998-08-18 to 1998-09-01 (14 days).

3.4 Mean Precipitation

Table 1 shows the total surface rain rates, averaged over the 14 days period and the model domain. The rain rates of the NASA TMI (.193 mm/h) and PR (.148 mm/h). Products differ by about 25 %. The REMO model rain rates (.246 mm/h) are 20 % higher than the highest (TMI) satellite estimate. Thus the model rain-rates are certainly too high.

Product			rain rate [mm/h]	percentage conv.	percentage no rain	number of pixels	number of events
REMO	regional model	MPI	.246	86%	70%	741393	113
REMO	coincident with TMI	MPI	.242			100007	88
REMO	coincident with PR	MPI	.244			30007	81
TMI	2a12, Version 4	NASA	.193		74%	100007	88
PR	2a25, Version 4	NASA	.148	52%	62%	30007	81
TMI		IFA	.107			33283	30
TMI	TMI only	DLR	.123			87274	82
TMI	TMI calibrated by PR	DLR	.116			87274	82
PR	Adjusted Z-R	CETP	.210			27840	75
PR	Constant k-R	CETP	.180			27840	75
SYNOP	gauge measurements	GPCC	.147			4584	105
SYNOP	interp.gauge(Kriging)	GPCC	.184			30247	73
GPCP 1DD	satellite + gauge	GPCC	.179			688905	105

Table 1: Mean surface rain rates averaged from 1998-08-18 to 1998-09-01. Data was used from the from the EuroTRMM project partners: Centre d'Environnement Terrestre et Planétaire (France, CETP), German Aerospace Research Establishment (Germany, DLR), Istituto di Fisica dell'Atmosfera (Italy, IFA), Max Planck Inst. for Meteorologie (Germany, MPI), Global Presipitation Climatology Centre (Germany, GPCC).

NASA Version 4 data has been used for this comparison. In the meantime Version 5 is available for this period but could not be included in this comparison. In Version 5 TMI and PR rain rate estimates are more consistent.

The rain rate estimates provided by the EuroTRMM project partners are given in the third section of Table 1. The PR algorithms from CETP give higher rain-rates than the NASA product and more support the TMI estimates. The TMI algorithms from DLR and IFA use databases of cloud resolving model results, which to a large degree consist of hurricane simulations. This may be the reason for the low estimates provided by them in this case study with only moderate rain rates.

The last section of Table 1 shows total rain rates derived from gauge measurements. Raw SYNOP gauge measurements provide relatively low rain rates. These measurements are not representative because the rain gauge stations are unevenly distributed. Interpolation (Kriging) within an influence radius of about 100 km gives higher weights to observations in data sparse regions and provides higher rain-rates. The GPCP 1° daily merged satellite and gauge estimate is an operational (still experimental) product. This product provides a rain rate of .179 mm/h which is comparable to NASA TMI estimates.

The percentage of convective rain and the percentage of pixels with no rain is given in the second column of Table 1. Convective rainfall amounts to 86% in the model whereas PR estimates about 52%.

As shown in the last two columns the number of pixels and events contributing to the average is quite different depending on the instrument used. (An event denotes availability of data within the 3 hours output interval of the model. The numbers are smaller for PR than for TMI because the swath is narrower. TMI estimates from IFA and DLR are only provided over sea. IFA TMI and GPCC interpolated gauge measurements were not provided for the whole time interval). In order to justify the comparison in view of the different statistical base of the data sets REMO rain rates also have been accumulated only for events coincident with TMI and PR over-passes. The main results are not changed when using this restricted data set.

3.5 Sensitivity Studies

According to the findings in the previous Section, REMO produces too much rain in the Pacific atoll case study. A number of sensitivity experiments has been conducted in order to identify parameters responsible for this overestimation. Most experiments have only little influence on the observed rain rates (mean, profiles and intensity distributions). The mean surface rain rates and the percentage of convective rain, for cases substantially different from the control run, are given in Table 2. The second of the two weeks of model integration is considered here, because the model needs some time to adapt for some of the parameter changes.

Exp.	rain rate [mm/h]	conv.	parameter changed	in Eq.	meaning
reference					
2A12	.206				NASA TMI Version 4
2A25	.164	47%			NASA PR Version 4
e041	.253	84%			REMO reference run
changed parameters					
e028	.238	84%	$\tau = 1800$s	(9)	convective adjustment time increased
e032	.223	52%	$\epsilon_u = 4.e\text{-}4$	(6)	turbulent entrainment rate increased
e037	.227	44%	$\delta z_b = 3000$m	(5)	min. level above cloud base for convective rain
e030	.216	100%	lkon = F		condensation switched off
changed boundary conditions					
e033	.203	85%	$q = q \times 0.9$		reduced water vapour in b.c.
e035	.156	74%	$T_s = T_s$ - 1.K		reduced sea surface temperature
e040	.200	82%	$\beta = 0.0008$	(11)	increased transport for free convection

Table 2: Mean surface rain rates in the Pacific atoll region from August 25 to September 1, 1998 for REMO model runs with changed parameters.

Although some changes are large and probably unrealistic the mean surface rain rate only changes slightly. The percentage of convective rain is affected more. Even switching off convection totally, decreases the total rain rate by only 13%. The mean rain rate is primarily constrained by the moisture supply provided by the external forcing at the lateral boundaries and the latent heat flux at the lower boundary.

In order to investigate the influence of the boundary conditions, model runs were performed with i) decreased water vapour content in the initial state and at the lateral boundaries, ii) with decreased sea surface temperature, and iii) with a change in the parameterization in case of free convection (i.e. in case of low wind speeds). Reduction of the water vapour content by 10% leads to a degrease of the rain rate averaged over the whole domain rates by 20% which would be required to meet the observations, but the reduction mainly stems from a limited region near the inflow boundary. In the inner of the domain the original amount of water vapour has recovered and the precipitation rate remains the same.

The other source of moisture is the sea surface. The sea surface temperatures were prescribed from the ECMWF analyses as well. If sea surface temperature is decreased by 1 K the rain rate decreases by 40%. Thus a decrease by 0.5 K is required in order to get results comparable to the observations.

On the other hand the formulation of the lower boundary condition influences the flux of latent heat i.e. the moisture flux from the surface. The most sensitive parameter influencing the total rain rate is β (Eq. 11) which determines the amount of turbulent transfer at the surface in the free convection limit (for low wind speeds). Parameters of the convection scheme itself only have limited impact on the total rain rate. Their influence on profiles and rain intensity distributions is discussed in the following sections.

3.6 Frequency Distributions of Rain Rate Intensities

Satellite observed rain rates are instantaneous values and thus should be compared to instantaneous model rain rates as far as distributions of rain rate intensities are concerned. The instantaneous model rain rates (Figure 4) peak at a high value whereas the satellite derived rain rate distributions are much broader. The convection scheme obviously produces too high and too uniform rain rates. The 3 hourly accumulated rain rates correspond better with the satellite estimate, but the distribution is still too narrow. The rain rate distribution estimated from the PR is more flat than that from TMI and shows more rain with low intensities as already seen.

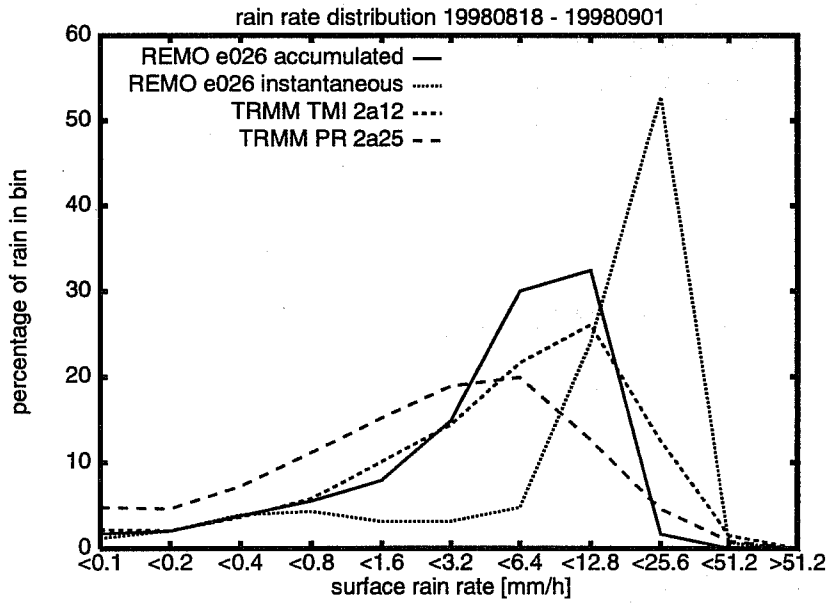

Figure 4: Frequency distribution of rainfall rates from August 18 to September 1 in the Pacific atoll domain for the REMO model and the TRMM precipitation estimates. Rain-rates have been aggregated on the $1/2^o$ grid of REMO before calculating the distributions. The percentage of rain within each class of rain rate intensities (logarithmic scale) is shown.

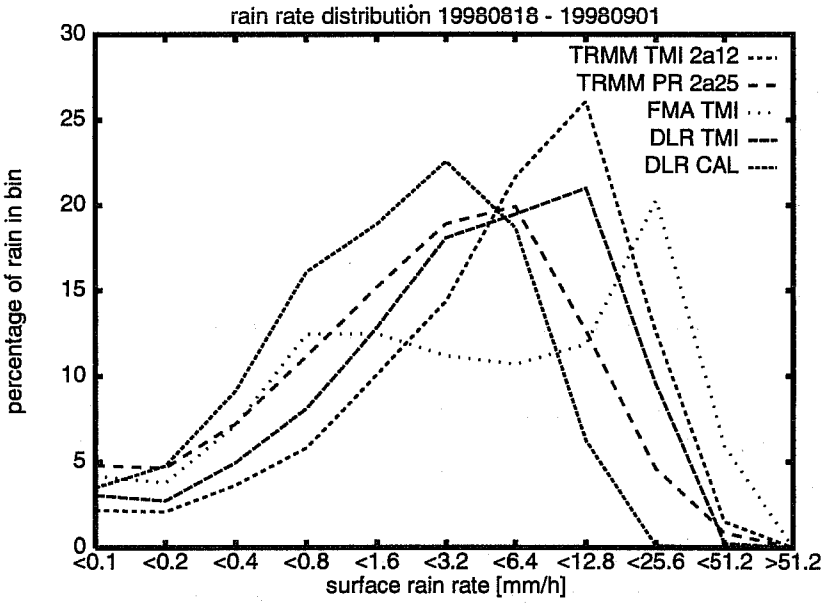

Figure 5: As figure 4 but for the EuroTRMM TMI estimates.

The frequency distribution of rainfall rates from the different TMI retrieval algorithms is shown in Figure 5. The DLR algorithm shows a flatter distribution than the 2A12 algorithm, comparable with that from the PR. The DLR calibrated approach leads to a distribution shifted to lower values. The IFA algorithm is the only one that shows a bimodal distribution similar to the instantaneous model precipitation, but it cannot be judged if this is a realistic feature. The distributions from the CETP PR estimates (not shown) are very similar to those from 2A25 but slightly shifted to higher values.

3.7 Profiles

The TRMM precipitation radar can provide estimates on vertical profiles of rainfall rates. In the model the diagnosed precipitation rate profiles are related to the vertical distributions of heating and drying in the atmosphere as shown in Figure 6. The sources of rainfall are very closely related to the respective heating and drying rates for the stratiform convection. The relation is much more indirect for the convective precipitation. Vertical transport and parameterized processes as entrainment and detrainment contribute substantially to the vertical distribution heating and drying rates felt by the atmosphere on the model grid-scale. Especially drying is highest at the lowest model levels well below the origin of precipitation.

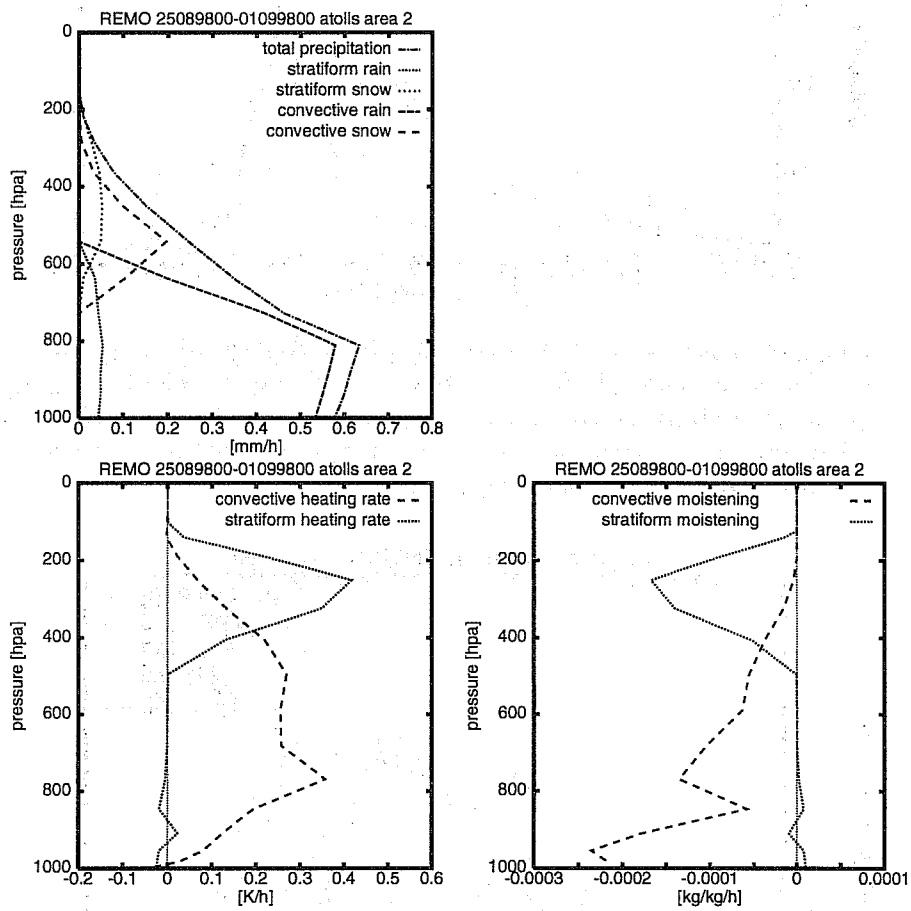

Figure 6: Profiles of stratiform and convective model precipitation rates (top), and the associated heating rates (bottom left, without the contribution of melting snow) and moistening rates (right).

Figure 7 (top) shows the mean stratiform and convective profile, as estimated from the PR. Because the number of stratiform events is much higher, approximately the same amount of precipitation is classified as convective and stratiform, despite the different amounts of rain rates shown in the figure.

Figure 7 (middle left) shows the REMO precipitation profile from the standard parameterization for comparison with the PR. The model precipitation rates reach up far into the troposphere with a considerable contributions from the ice phase, whereas PR rain rates almost vanish above 6000 m. The estimation of rain-rates from measured backscatter profiles strongly depends on assumptions on micro-physical properties (e.g. droplet size distributions, ice properties). Because PR radar works only with one frequency there is no mean to get this information from the measurements itself. Especially in the ice phase (and in the melting layer in case of stratiform rain) the uncertainties are large. Near the ground the signal cannot be interpreted due to surface backscatter.

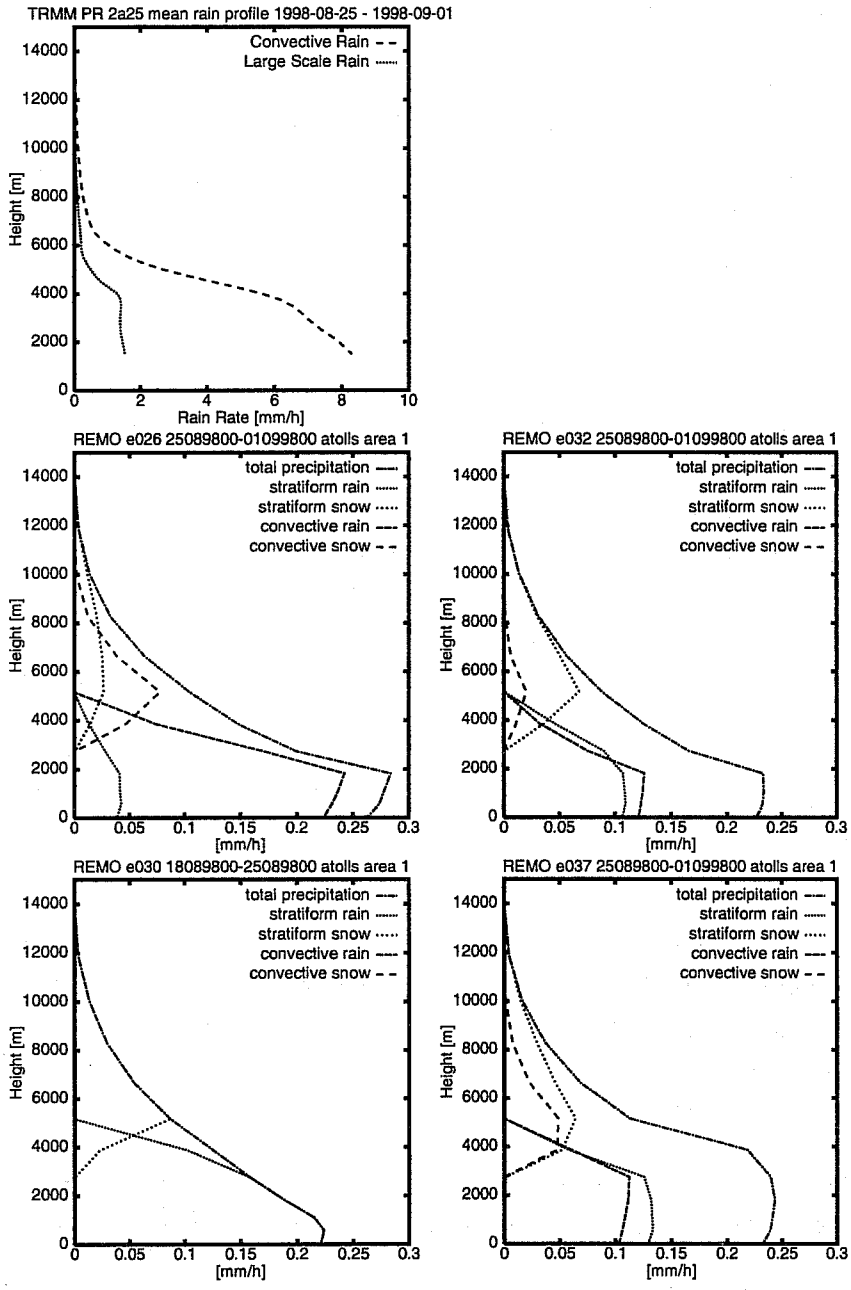

Figure 7: Mean stratiform or convective precipitation profiles estimated from TRMM PR (top) and average stratiform or convective rain rates for different choices for parameter values in the convection scheme (middle left to bottom right): Standard parameter settings, entrainment rate increased to $\epsilon_u = 4 \times 10^{-4} m^{-1}$, convective rain switched off, threshold level δz_b increased from 1500m to 3000m

In the height range which is well covered by the PR the stratiform precipitation profile does not show much variation whereas the convective profile continuously increases towards lower levels. This behavior is present both in the observations and in the model results. In contrast to the observations the modeled profile shows a distinct maximum at 2000 m height.

The remaining panels show profiles from model runs with strong changes made to some parameters. In the top middle panel the entrainment rate was enhanced. This prevents convection to reach as high as in the standard case. The convective part of precipitation is decreased whereas the stratiform rain increases. The profile of total rain rate does not change very much. Even if the convective rain is switched off totally (bottom left) the stratiform rain overtakes its part so that the profile of total rain again approximately remains constant.

The convective precipitation profile has a pronounced maximum just below 2000m. This maximum is directly related to the parameter δz_B = 1500m in the cumulus parameterization. Below this level convective precipitation is suppressed. if this level is lifted to δz_B = 3000m the shape of the precipitation profile changes considerably (cf. bottom right panel).

4. Conclusions

Precipitation fields from the mesoscale model REMO in the Pacific atoll region were compared to the rain rate estimates derived from TRMM for a two weeks period in order to evaluate the model parameterizations. The spatial distribution of rain rates corresponds very good with those from the model. The observational estimates of the mean rain rates from PR and TMI for the whole period differ by about 30% (for NASA Version 4 products). Model rain rates are 20% higher than the highest estimate and thus are certainly too large. In the model convective rain contributes with 86% to the total rain-rate, which is regarded as a reasonable value in the tropics, whereas in the PR retrievals only 52% of the rain is classified as convective.

Parameters of the convection scheme itself have little influence on the total amount of rain. Rain rates are mostly determined by the lower boundary conditions, namely sea surface temperature and the parameterization of turbulent transfer of sensible and latent heat from the sea surface. This part of the model physics provides the parameters with the highest impact on total rain rates.

The uniqueness of TRMM is that it provides information on vertical profiles of precipitation. The accuracy of rain rate estimates derived from the PR backscatter using only one frequency, is limited by the lack of knowledge of droplet distributions and by the properties of hydrometeors in the ice and melting phase. Modelled precipitation profiles show a distinct maximum at 2000 m, depending strongly on a certain parameter (δz_B) in the convection parameterization.

Histograms of modeled instantaneous rain rate intensities show a narrow peak at high rain rates, caused by the convection parameterization. The distribution of observed rain rates is much broader.

In the past, model parameterizations were designed to give reasonable rain rates for the climatological mean or diurnal cycle and reasonable distributions of heating and moistening rates. Precipitation profiles or accurate instantaneous rain rates were not really considered. Thus it cannot be expected that these features are reproduced very well in the model. As more accurate observations become available, these aspects will gain more attention.

This case study focussed on mean rain rates, mean precipitation profiles, and distributions of rain rate intensities. Other aspects of the data as for instance the exact time and location of precipitation events, or the diurnal cycle of rain fall, were not considered. They will be more important for other case studies as hurricane development and precipitation over land.

References

Louis, J.F. (1979): A parametric model of vertical eddy fluxes in the atmosphere. *Bound. Layer. Meteor.*, **17**, 187-202

Miller, M.J., A.C.M. Beljaars and T.N. Palmer (1992): The sensitivity of the ECMWF model to the parameterization of evaporation from tropical oceans. *J. Climate*, **5**, 418-434

Nordeng, T.E. (1994): Extended versions of the convection parameterization scheme at ECMWF and their impact upon the mean climate and transient activity of the model in the tropics. *Research Department Technical Memorandum* No.206, ECMWF

Roeckner, E., K. Arpe, L. Bengtsson, M. Christoph, M. Claussen, L. Duemenil, M. Esch, M. Giorgetta, U. Schlese (1996): The atmospheric general circulation model ECHAM-4: Model description and simulation of present-day climate. *Max-Planck-Institut fuer Meteorologie, Report* No. 218.

Sundquist, H. (1978): A parameterization scheme for non-convective condensation including prediction of cloud water content. *Quart. J. R Met. Soc.*, **104**, 677-690

Tiedtke, M. (1989): A comprehensive mass flux scheme for cumulus parameterization in large-scale models. *Mon. Wea. Rev.*, **117**, 1779-1800